ACS OMEGA

Open Access

http://pubs.acs.org/journal/acsodf

Article

Phase Change Materials for Energy Storage Applications from PEG and PBAT with AlN and CNT as Fillers

Eyob Wondu,[‖] Wondu Lee,[‖] Minsu Kim, Dabin Park, and Jooheon Kim*

Cite This: *ACS Omega* 2024, 9, 49557−49565

Read Online

ACCESS | Metrics & More | Article Recommendations | Supporting Information

ABSTRACT: This study investigates the fabrication of phase change material−poly(butylene adipate-*co*-terephthalate) (PCM−PBAT) composites through melt blending techniques, focusing on the impact of isophorone diisocyanate (IPDI) treatment on carbon nanotubes (CNTs) and (3-aminopropyl)triethoxysilane (APTES) treatment on aluminum nitride (AlN) particles. Analysis of mechanical properties highlights an enhancement in tensile strength with APTES-treated AlN particles, while dynamic mechanical analysis (DMA) reveals an increase in stiffness. Laser flash analysis (LFA) investigation demonstrates a significant increase, up to 325%, in thermal conductivity compared to PCM−PBAT composites without filler. Moreover, the fabricated composites exhibit enhanced latent heat storage capabilities, with the PCM−PBAT composite containing 30% filler (20PCM−PBAT−30F) showing promising latent heat values. These findings underscore the efficacy of selecting an appropriate PCM−PBAT ratio and surface functionalization of the filler particles in enhancing the latent heat storage and thermal and mechanical properties of the polymer composites, suggesting their potential application across diverse fields.

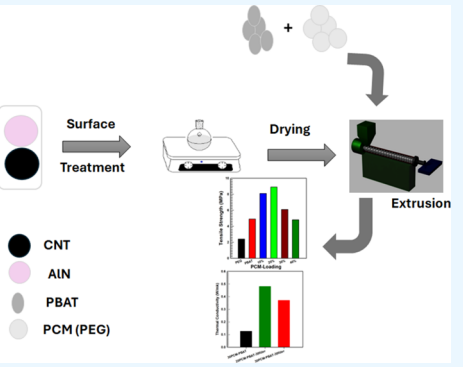

1. INTRODUCTION

Sensible heat, thermomechanical reaction energy, and latent heat are the three types of energy storage mechanisms for thermal applications.[1] Currently, among these thermal energy storage mechanisms, latent heat is predominantly utilized, with phase change materials (PCMs) playing a crucial role in this domain.[2−7] Latent heat storage, which utilizes PCMs to store or release latent heat, finds diverse applications, including the recovery of industrial waste heat, building comfort systems, cooling, and temperature control systems.[6] Among PCMs, poly(ethylene glycol) (PEG) is distinguished for its high energy storage density, suitable phase change temperature, stability, low toxicity, and cost-effectiveness.[8−10] However, inherent limitations, such as leakage in the molten state, low thermal conductivity, and significant supercooling, restrict its practical applications, leading to thermal response hysteresis and reduced energy storage and thermal regulation performance.[6,9,11] Addressing these challenges may be feasible through packaging techniques and the incorporation of fillers with high thermal conductivity.[12−15]

For this purpose, materials that exhibit high thermal conductivity,[11,16−19] including ceramic fillers (such as boron nitride (BN),[20,21] aluminum nitride (AlN),[22,23] and alumina (Al_2O_3)),[24,25] carbon-based fillers (like graphite, graphene, and carbon nanotubes),[16,18,25−27] and metals (such as copper, iron, and silver)[28,29] are integrated into polymer matrices to fabricate composites with enhanced thermal conductivities. However, it is acknowledged that a higher percentage of filler loadings might compromise the properties of the composites by introducing defects that impede their thermal dissipation performance, especially under conditions of vibration and shock in devices.[19,30,31] Consequently, achieving high thermal conductivity with a lower percentage of filler loading remains crucial for the functionality of these composites. Despite numerous efforts to enhance the thermal conductivity of polymer composites through various methods such as freeze-casting, functionalization, and chemical vapor deposition, the challenge persists. An intriguing approach for effective thermal management involves using PCMs as the matrix in conjunction with other polymer materials. PCMs, such as paraffin, PEG, and erythritol, show promise for heat energy storage due to their significant latent heat capacity, offering potential for energy conservation and heat regulation.[4] Consequently, research efforts are directed toward integrating PCMs into thermally conductive polymer composites.

While numerous studies have sought to enhance thermal management using PCM materials, certain challenges persist. First, the high filler loadings required to increase the thermal conductivity of composites often diminish the latent heat capacity of PCMs, necessitating a balance between retaining

Received: August 13, 2024
Revised: November 22, 2024
Accepted: November 26, 2024
Published: December 6, 2024

Scheme 1. Methodology[a]

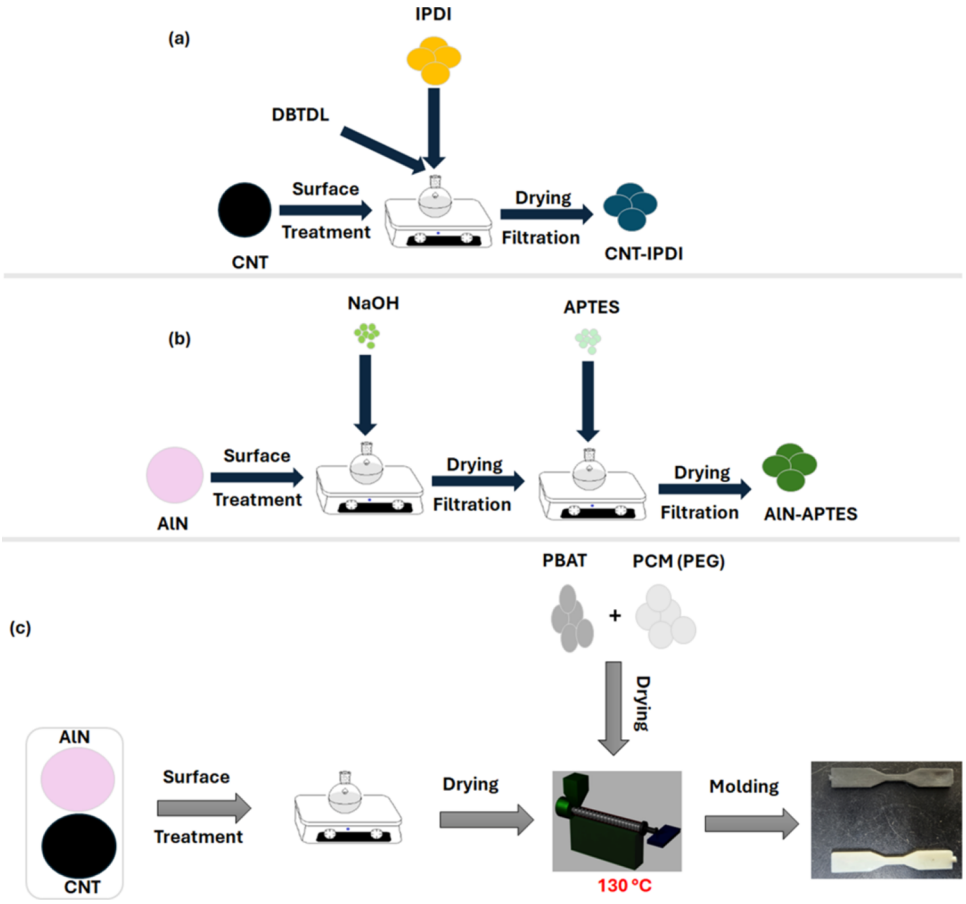

[a](a) Schematic illustration of the surface modification of CNT with IPDI, (b) surface modification of AlN with APTES molecules, (c) schematic illustration of the fabrication of the various composites of PCM−PBAT−filler matrix.

intrinsic latent heat and improving thermal conductivity.[2,4−6] Second, the mechanical properties of commonly used PCMs, like paraffin, typically fall short of those of common polymers found in thermally conductive composites, such as epoxy,[32,33] polyurethanes,[24] and poly(vinyl alcohol) (PVA).[34] The main problem encountered while utilizing these polymers together with the PCM is that the melting point of the two varies widely. Thus, considering a polymer having a low melting point but good mechanical properties like poly(butylene adipate-terephthalate) (PBAT) is suitable to process the PCM-polymer composites.[35] This mechanical fragility in PCMs poses a barrier to their practical implementation, underscoring the importance of enhancing the mechanical properties of PCMs for applications in electronic devices.

Considering the challenges in previous research works in heat management of PCM applications, such as leakage in the molten state, low thermal conductivity, and significant supercooling that limit their practical use, this study proposes a novel approach for fabricating a PCM composite from PEG and PBAT aimed at achieving a composite with high latent heat capacity and promising thermal conductivity without compromising the mechanical properties of the final composites. To this end, aluminum nitride (AlN) and carbon nanotubes (CNTs) are employed to enhance thermal conductivity and latent heat capacity without altering the mechanical properties of the composites. The PCM composites obtained in this study demonstrate promising latent heat and heat dissipation characteristics.

2. EXPERIMENTAL SECTION

2.1. Materials. PEG (molecular weight of 20,000, melting point of 59−65 °C), sodium hydroxide (NaOH), and ethanol (95%) were obtained from Dae-Jung Chemical and Metal Co., Ltd. (Seoul, Korea). The thermoplastic polymer PBAT (melting point 120−140 °C) was acquired from Dong-Sung Chemical (Ulsan, Korea). AlN (10 μm, 98%), CNTs, isophorone diisocyanate (IPDI), dibutyltin dilaurate (DBTDL, catalyst), and (3-aminopropyl)triethoxysilane (APTES, 95%) were procured from Sigma-Aldrich (Minnesota).

2.2. Methods. The surface reactivity of CNTs and AlN particles was insufficient for effective bonding with the PCM−PBAT matrix. Therefore, enhancing their surface properties was crucial to facilitate proper adhesion and compatibility with the PCM−PBAT matrix. To address this issue, IPDI was introduced to the surface of CNTs using DBTDL as a catalyst. Initially, CNTs were mixed in acetone solvent through stirring, and IPDI was added to the solution, followed by the simultaneous addition of the DBTDL catalyst dropwise. The resulting mixture was placed in an oil bath at 60 °C while stirring, and the reaction was sustained for 8 h. IPDI, constituting 10 wt %, relative to the weight of the CNTs, was added to the solution for the surface treatment of CNTs.

https://doi.org/10.1021/acsomega.4c07480
ACS Omega 2024, 9, 49557−49565

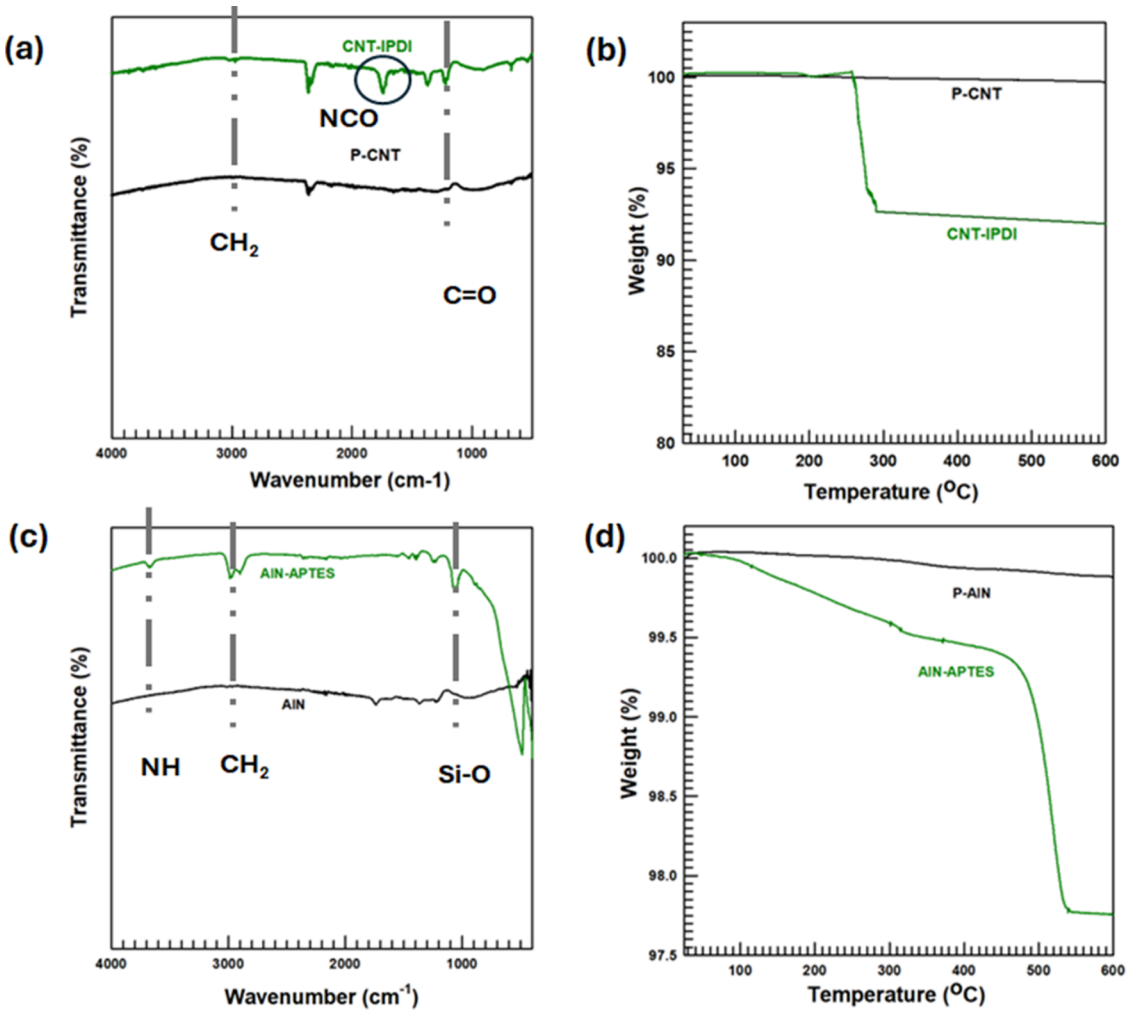

Figure 1. Confirmation of surface treatments: (a) FTIR; (b) TGA of IPDI-treated CNT, respectively; (c) FTIR; and (d) TGA of APTES-treated AlN particles.

Subsequently, the IPDI-treated CNTs were separated from the solution through vacuum filtration. The surface functionalization of CNT particles is detailed in Scheme 1a.

Furthermore, the AlN particles were surface-functionalized through APTES functionalization. To enable surface treatment with APTES, the particle should possess a hydrophilic component capable of reacting with the silane groups of APTES molecules. Considering the lack of hydroxyl groups on AlN, its surface was initially subjected to a hydroxyl group treatment using NaOH as the source of OH groups. A 3 M NaOH solution was prepared, and the AlN particles were mixed into this solution while stirring. The attachment of hydroxyl groups to the surface of AlN occurred over 24 h in an oil bath at a temperature of 80 °C. Finally, the basic solution was neutralized from the AlN particles by washing with deionized water (DI) and filtration, and the filter cake was subjected to drying for 24 h at 60 °C. Upon drying, the cake underwent APTES treatment (5 wt % with respect to AlN) by dissolving the OH-attached AlN particles in an ethanol solvent. The reaction took place in an oil bath at a temperature of 80 °C, stirring for 6 h. Finally, the solution was separated from the solvent through filtration, and the filter cake was dried in an oven at 60 °C for 24 h. The schematic representation of APTES surface functionalization of AlN particles is illustrated in Scheme 1b.

Once the surface functionalization of the filler particles is achieved such that the diisocyanate group reacts with the PEG (PCM) and the silane-containing AlN reacts with the IPDI molecules functionalized on the surface of the CNTs, the preparation of the PCM−PBAT−filler composite followed. The melt blending technique was used to fabricate the composite materials, followed by pelletizing and molding into proper shapes for analysis.

Prior to fabricating the composite containing the filler particles, a proper PCM−PBAT mixing ratio was determined producing various PCM−PBAT composites and evaluating its effect on the mechanical properties. PCM ratios ranging from 10 to 40 wt % were mixed with corresponding PBAT, melt extruded, and their mechanical properties were examined. Through this evaluation, the optimal ratio of PCM to PBAT was determined to be 20PCM−PBAT (20 wt % PCM and 80 wt % PBAT). To fabricate the composites, a constant 3 wt % CNT relative to the 20PCM−PBAT matrix was used, and 27 wt % of AlN was applied and labeled as 20PCM−PBAT−30F. For comparison purposes, a 30PCM−PBAT composite (30 wt % PCM and 70 wt % PBAT) was also melt extruded with the same ratio of CNT and AlN and labeled as 30PCM−PBAT−30F. The melt blending temperature was set at 130 °C with an extrusion speed of 83 rpm. Atmospheric air was used to cool the extrudate, as water dissolves the PCM. The schematic

https://doi.org/10.1021/acsomega.4c07480
ACS Omega 2024, 9, 49557−49565

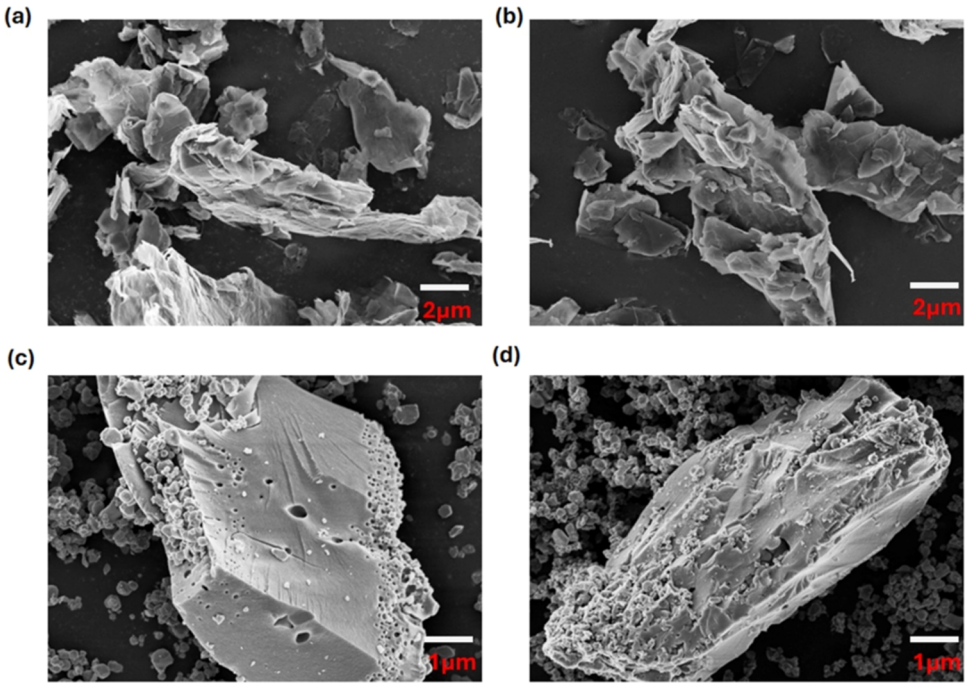

Figure 2. Adhesion properties of surface treatments of fillers: (a) pristine CNT; (b) IPDI-treated CNT; (c) pristine AlN; and (d) APTES-treated AlN.

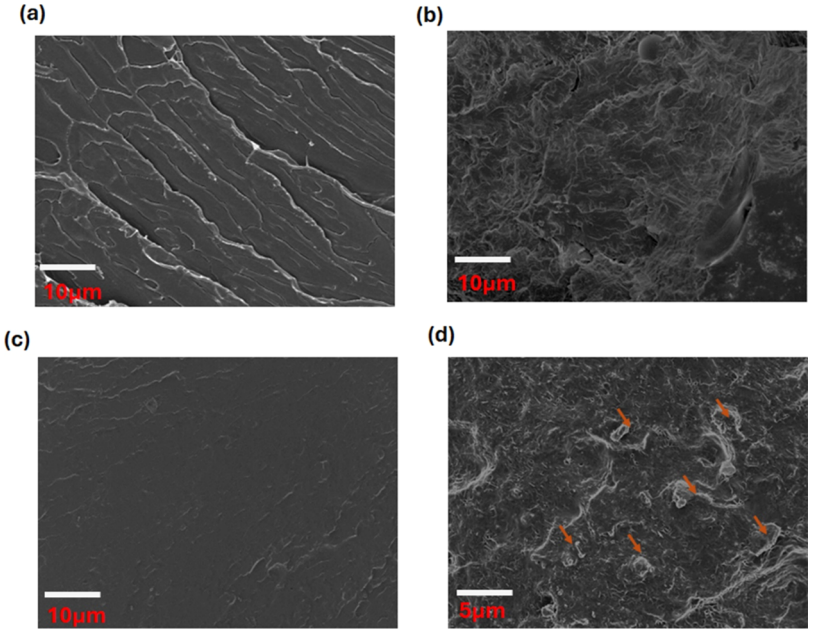

Figure 3. Morphology of various composites: (a) neat PBAT; (b) PEG (PCM); (c) 20PCM−PBAT; and (d) 20PCM−PBAT−30F.

illustration of the fabrication of the composite is displayed in Scheme 1c.

2.3. Characterization. The characterization methods applied in this study are stated in the Supporting Information.

3. RESULTS AND DISCUSSION

In this study, the impacts of IPDI treatment on CNTs and APTES treatment on AlN particles were examined using various analytical methods, including TGA, FE-SEM, and FTIR spectroscopy. These techniques were utilized to assess the chemical and physical alterations in the particles subsequent to the treatments. FTIR analysis of the IPDI-treated CNT particles, as depicted in Figure 1a, revealed the presence of NCO, methylene, and carbonyl groups on the particle surfaces, indicated by peaks at 1740, 2950, and 1100 cm^{-1}, respectively. These functional groups are attributed to the IPDI molecules, which contain NCO, methylene, and carbonyl groups, due to the introduction of isocyanate groups on the surface of the CNTs that are not present in the pristine CNT (P-CNT). Similarly, the FTIR spectra of APTES-treated AlN particles, shown in Figure 1c, exhibited distinctive peaks corresponding to methylene, NH, and silane groups at 2950, 3400, and 1280 cm^{-1}, respectively. These observations are distinct from the pristine AlN particles (P-AlN) suggesting the

https://doi.org/10.1021/acsomega.4c07480
ACS Omega 2024, 9, 49557−49565

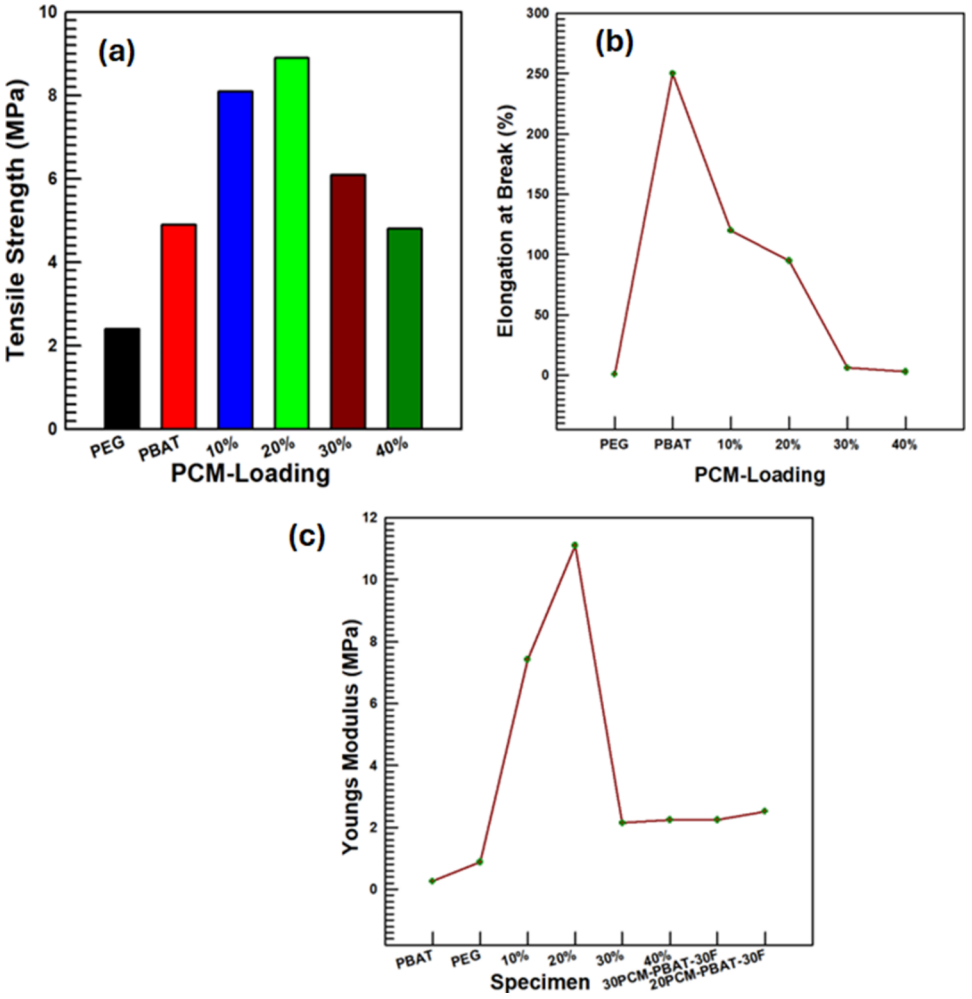

Figure 4. UTM investigations: (a) tensile strengths; (b) elongation at break; (c) Young's modulus of various PCM loadings in the PBAT matrix and the corresponding filler loadings.

successful functionalization of particle surfaces with APTES groups.

The TGA results for IPDI-treated CNT and APTES-treated AlN particles, presented in Figure 1b,d, respectively, offer insights into the thermal stability and degradation profiles of the treated particles. The IPDI-treated CNTs displayed an onset of degradation at 210 °C, attributed to the degradation of IPDI groups, with a significant degradation observed at temperatures exceeding 288 °C, where approximately 8 wt % of the CNTs underwent thermal degradation (Figure 1b).

This finding indicates the treatment of CNT surfaces with IPDI groups. Contrastingly, pristine AlN particles showcased high thermal stability with no observable degradation, even at elevated temperatures. However, the APTES-treated AlN particles began degrading at lower temperatures, with complete degradation of the reacted APTES groups occurring around 510 °C, leaving behind residual AlN particles (Figure 1d). The degradation resulted in a loss of approximately 2.3 wt %, suggesting that the APTES attached to the AlN particles constituted 2.3 wt %, with an additional 2.7 wt % possibly attributed to unreacted APTES, given that 5 wt % APTES was used for the surface treatment of the AlN particles.

Moreover, the surface morphology modifications observed in the FE-SEM images (Figure 2) indicate that the surface of CNTs and AlN particles has been improved upon the introduction of IPDI and APTES molecules. The pristine CNT (Figure 2a) indicates a surface having a thin structure with rods on it, whereas the IPDI-treated CNT (Figure 2b) displays a smooth surface with dots on it which corresponds to IPDI molecules distribution over the surface of CNT. In addition to this, the TEM images displayed in Figure S1 reveal the presence of a rodlike structure for the IPDI-treated CNT. The EDS analysis also confirms the presence of N ascertained from NCO groups used to treat its surface. Pristine AlN (Figure 2c) has a smooth surface morphology with pores, whereas the APTES-modified AlN particles (Figure 2d) have a rough surface morphology having APTES molecules well distributed over the surface of AlN particles. Furthermore, the presence of APTES molecules is confirmed by EDS analysis displayed in Figure S2. The presence of Si elements does confirm that APTES molecules are attached to the surface of AlN particles.

FE-SEM images in Figure 3a–d elucidate the surface morphologies of various fractured specimens. The neat PBAT displayed a fractured, ladder-like morphology, indicative of a ductile nature (Figure 3a), which was altered upon the inclusion of PEG–PCM, known for its high brittleness. However, the PEG (PCM)'s morphology shows a porous material having a highly brittle property (Figure 3b).

https://doi.org/10.1021/acsomega.4c07480
ACS Omega 2024, 9, 49557–49565

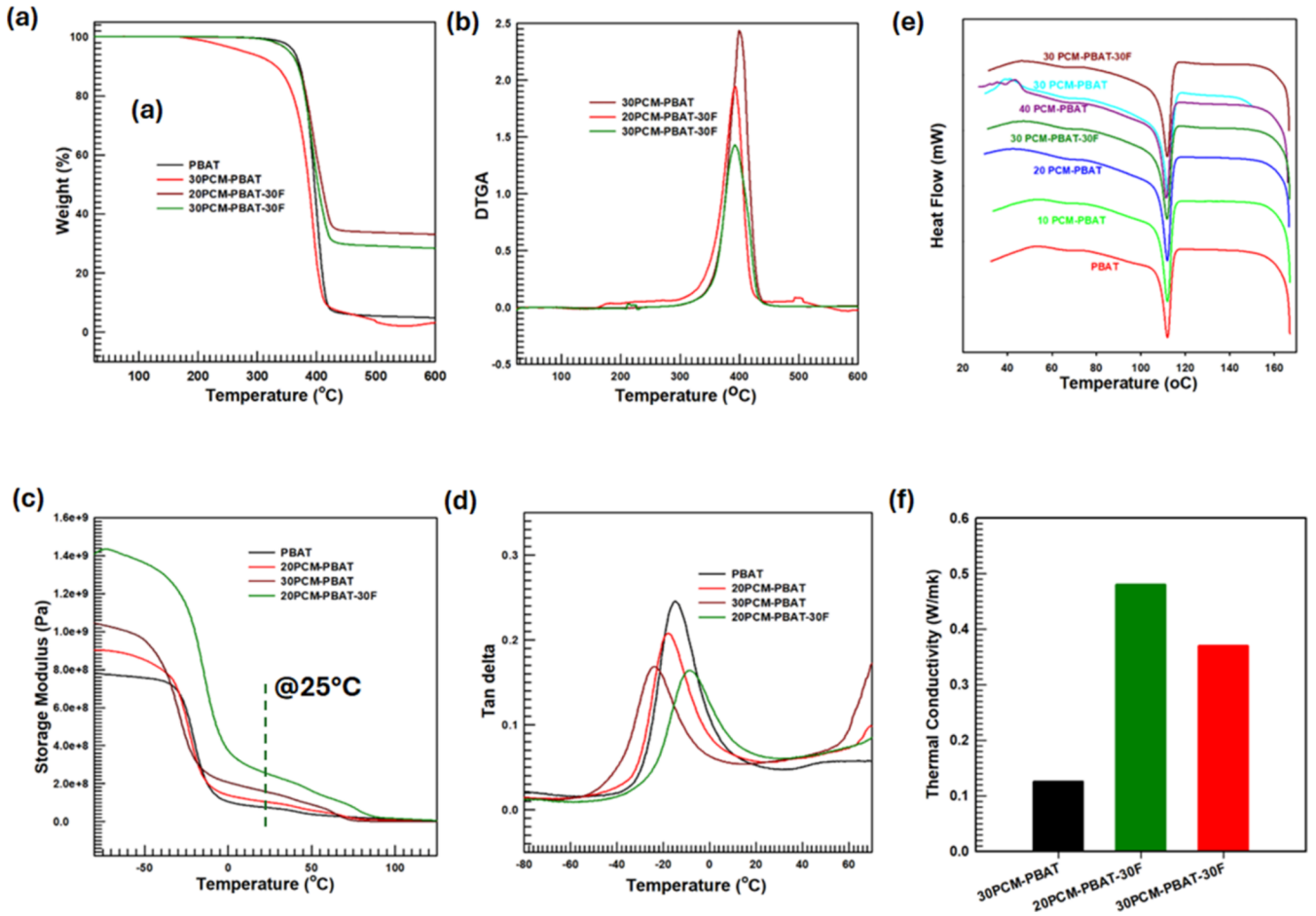

Figure 5. Thermal and mechanical properties of various composites: (a) TGA; (b) derivative TGA; (c) storage modulus; (d) tan δ; (e) heat flow; (f) thermal conductivity of PCM−PBAT and filler composites.

For comparison, the FE-SEM image of 20PCM−PBAT analyzed and depicted in Figure 3c exhibited a highly fractured specimen with a smooth structure, confirming its high brittleness but more ductile as compared to PCM, this analysis is supported by the UTM analysis. Figure 3d demonstrates that the APTES-AlN particles and IPDI-CNTs were well distributed in the PCM−PBAT matrix, indicating good interfacial adhesion between the filler particles and the PCM−PBAT blend. This compatibility is attributed to the APTES functionalization and the reaction between IPDI molecules and PEG−PCM.

The mechanical properties of the various PCM−PBAT composites were investigated using UTM results, as illustrated in Figure 4. Neat PBAT exhibited an average tensile strength of approximately 5.2 MPa, while neat PEG, used as the PCM, exhibited a tensile strength of 2.1 MPa. The tensile strength of the various PCM−PBAT composites, used to determine the optimal ratio of PCM to PBAT in the matrix, is presented in Figure 4a. As the ratio of PCM (PEG) increases, the tensile strength initially increases but then decreases drastically upon reaching a threshold level. The 20PCM−PBAT composite achieved the highest tensile strength of all fabricated composites at 8.8 MPa. Although the tensile strength increases with the addition of PCM to the PBAT matrix, the elongation at break decreases once PCM is introduced, resulting in an elongation at break of 250% for neat PBAT and 2% for PEG. The 10PCM−PBAT exhibited an elongation at break of approximately 110%, reflecting the highly brittle nature of PEG PCM, with this property decreasing upon increasing the PCM ratio, as shown in Figure 4b.

Conversely, the Young's modulus, as depicted in Figure 4c, exhibited a different trend, with PBAT having the lowest Young's modulus of around 0.5 MPa and PEG achieving 0.8 MPa. Mixing the PCM (PEG) with the PBAT matrix significantly improved Young's modulus until it reached a threshold level. The 20PCM−PBAT displayed a Young's modulus of 11.8 MPa, after which it decreased. These properties indicate that the optimal ratio of PCM to PBAT is achieved with 20PCM−PBAT, which is considered optimum as it presents a tensile strength of 8.8 MPa, 95% elongation at break, and Young's modulus of 11.8 MPa. The Young's modulus of 20PCM−PBAT−30F has shown a drop from the 20PCM−PBAT due to the inclusion of filler particles that has deteriorated the mechanical property; the same applies for the 30PCM−PBAT−30F. For comparative purposes, the 30PCM−PBAT was also used in this study. Moreover, the inclusion of APTES-AlN particles led to an increase in tensile strength, peaking at around 10.1 MPa, as shown in Figure S4. The stress−strain diagram of 20PCM−PBAT−30F and 30PCM−PBAT−30F is displayed in Figure S4a, which showcases a huge difference between the two considered. 20PCM−PBAT−30F's stress−strain diagram shows a material with higher strength and elongation at break with it retaining the elongation at break for a while as compared to 30PCM−

https://doi.org/10.1021/acsomega.4c07480
ACS Omega 2024, 9, 49557−49565

PBAT−30F. Conversely, the 40PCM−PBAT polymer blend exhibited the lowest tensile strength at 4.8 MPa among all specimens, also having the lowest elongation at break of 3%.

However, the tensile strength of PCM−PBAT composites improved with the addition of AlN particles, with the strength at the breakpoint increasing proportionally to the quantity of AlN particles incorporated into the matrix. The composite with 20PCM−PBAT−30F demonstrated the highest tensile strength compared to 20PCM−PBAT but had a lower elongation at the break due to the inclusion of CNTs, which possess poor mechanical properties. Thus, while the inclusion of CNTs adversely affected the mechanical properties, the incorporation of AlN particles enhanced the strength at the breakpoint. The elongation at break of PCM−PBAT composites with filler particles is displayed in Figure S4c.

Thermal degradation results of the PCM−PBAT composites are presented in Figure 5a,b. Compared to neat PCM−PBAT, the incorporation of IPDI-treated CNTs and APTES-functionalized AlN particles enhanced the thermal stability of the PCM−PBAT composite. Neat PCM−PBAT underwent two thermal degradation stages: (i) degradation of the PEG segments in PCM−PBAT, initiating at 340 °C and continuing linearly up to 440 °C; (ii) further degradation of PBAT segments in PCM−PBAT, starting at 410 °C and extending linearly up to 585 °C, with less than 2 wt % residues. Thus, PCM−PBAT proves to be a thermally stable polymer. Conversely, the IPDI-treated CNT and APTES-functionalized AlN-PBAT composites exhibited a two-stage thermal degradation: (i) degradation of the PEG, alongside complete degradation of IPDI and APTES groups, occurring between 326 and 380 °C, (ii) degradation of PBAT segments together with remaining PEG between 400 and 575 °C, with the residues comprising CNTs and AlN particles. The superior thermal stability of PCM−PBAT, attributed to its higher glass transition temperature, as discussed in the DMA investigation, suggests its increased resistance to degradation or deformation under elevated temperatures. The improvement in thermal stability is confirmed by the derivative TGA (DTGA) in Figure 5b.

The dynamic mechanical analysis (DMA) results presented in Figure 5c,d shed light on the thermomechanical properties of various PCM−PBAT composites, incorporating IPDI-CNTs and APTES-AlN particles. The storage modulus (Figure 5c), which reflects the stiffness of each composite, and the glass transition temperature (Figure 5d), indicated by the tan δ value, are key metrics evaluated in this study. Neat PBAT exhibited the lowest storage modulus at room temperature, approximately 1.8×10^5 MPa. The addition of PCM to the PBAT matrix significantly improved the stiffness of the composites. The inclusion of AlN and CNT fillers, relative to the matrix including PCM and PBAT, increased the storage modulus at low temperatures (Figure 5c) and showed a similar trend at room temperature, with 20PCM−PBAT−30F exhibiting the highest stiffness, having a storage modulus of 3.9×10^5 MPa at 25 °C. Figure 5d illustrates the glass transition temperatures of various PCM−PBAT−filler composites. The inclusion of filler particles resulted in a rightward shift of the tan δ curve for each composite, indicating a higher glass transition temperature compared to neat PCM−PBAT. Conversely, PCM−PBAT composites without filler particles displayed a leftward shift in their glass transition temperature on the tan δ curve.

The crucial properties of PCM composites for application in heat dissipation materials is their latent heat or heat of fusion, which is derived from differential scanning calorimetry (DSC) spectroscopy. PEG (PCM) possesses an exceptional latent heat of 126 J/g, compared to the PBAT matrix, which has about half the latent heat of PEG. Mixing the two polymers increased the latent heat, although not satisfactory as significantly as desired when compared to PCM alone. The obtained latent heat, shown in Table 1, derived from the DSC curve (Figure 5e), offers a comparison of the heat of fusion of various fabricated composites. Increasing both the latent heat and thermal conductivity is crucial for the application of PCM composites in thermal energy storage.

Table 1. Latent Heat of the Fabricated Composites

sample	heat of fusion, J/g
PEG	126.4
PBAT	68.6
10PCM−PBAT	69.5
20PCM−PBAT	98.1
30PCM−PBAT	103.4
40PCM−PBAT	104.5
20PCM−PBAT−30F	122.07
30PCM−PBAT−30F	142.9

Remarkably, the inclusion of IPDI-functionalized CNT and APTES-functionalized AlN particles improved the latent heat of the PCM−PBAT matrix. The 20PCM−PBAT−30F composite demonstrated a 25% increase in latent heat at the melting temperature compared to 20PCM−PBAT. Although increasing the PCM loading enhances the latent heat, this approach adversely affects the mechanical properties, discussed in Figures 4 and S4, of the composites, making it an unsuitable alternative. Thus, the optimal ratio, as determined from the UTM analysis, is identified as 20PCM−PBAT. Coupled with the DMA analysis, which revealed a rightward shift of the glass transition temperature (Figure 5b) and the improvement in latent heat, the 20PCM−PBAT−30F composite shows promising results for applications requiring efficient thermal energy storage and management. The inclusion of the filler particles in the PCM−PBAT matrix has enhanced the latent heat even as compared to the PEG (30PCM−PBAT−30F has more latent heat than that of PEG PCM) which indicates the filler has improved the heat of fusion generated.

Leakage tests under increasing temperatures were conducted for various PCM−PBAT and PCM−PBAT−filler loadings. The results revealed that the 20PCM−PBAT−30F sample exhibited the highest resistance to heat-induced leakage, showing no leakage but some expansion at 160 °C. These findings are detailed in Figure S3. The PEG (PCM) melted and leaked at 90 °C within 1 min. However, incorporating the PBAT matrix mitigated this leakage problem at lower temperatures, as illustrated in the first row of Figure S3. Increasing the PBAT loading percentage further enhanced thermal resistance, even at temperatures above 90 °C. Conversely, neat PBAT melted and began leaking at a higher rate at 160 °C compared to PCM−PBAT. Adding AlN and CNT to the PCM−PBAT matrix improved resistance to induced heat. The specimen with a lower percentage of PCM (20PCM−PBAT−30F) showed no leakage and resisted heat-induced expansion at 160 °C more effectively than the

https://doi.org/10.1021/acsomega.4c07480
ACS Omega 2024, 9, 49557−49565

30PCM−PBAT−30F sample. Consequently, a leakage-resistant PCM−PBAT composite has been developed.

LFA was employed to assess the thermal conductivity of PCM−PBAT composite materials incorporating APTES-AlN and IPDI-CNT particles. Traditional polymer materials are known for their low thermal conductivity, typically exhibiting values below 0.2 W/(m·K). The thermal conductivity of composite materials is influenced by several factors, including the alignment of fillers within the polymer matrix, the presence of polymer chain defects, and voids. The thermal conductivity ((K)) of composite materials can be calculated using the equation

$$K = \rho C_p \delta \quad (1)$$

where ρ, C_p, and δ represent the density, specific heat capacity, and thermal diffusivity, respectively. The LFA machine determines the thermal diffusivity based on the sample thickness and diameter (12.5 mm), with C_p and ρ values provided to the machine.

This study explores the effect of incorporating APTES-functionalized AlN and IPDI-treated CNT particles into the PCM−PBAT polymer matrix on its thermal conductivity. The 20PCM−PBAT matrix, inherently nonconductive with a thermal conductivity of 0.12 W/(m·K), shows a significant increase in thermal conductivity upon the inclusion of APTES-functionalized AlN and IPDI-treated CNT particles. The bar graph depicted in Figure 5f illustrates a steep linear rise in thermal conductivity. By integrating 37 wt % APTES-functionalized AlN and 3 wt % of IPDI-treated CNT particles into the 20PCM−PBAT matrix, a remarkable enhancement of 325% in thermal conductivity is achieved compared to the neat PCM−PBAT matrix. This substantial increase is attributed to the synergistic effect of 3 wt % CNT combined with AlN particles, resulting in a total filler content of 40 wt % relative to the PCM−PBAT matrix, thereby enhancing the composite's ability to conduct heat.

4. CONCLUSIONS

In this study, the fabrication of various PCM−PBAT composites using melt blending techniques was investigated. We explored the effects of IPDI-treated CNTs and APTES-treated AlN particles through a range of analytical methods. FTIR and FE-SEM images are studied, and they demonstrate distinct functional groups on the surfaces of the treated particles and the particles were well dispersed within the PCM−PBAT matrix, respectively. The optimal ratio of PEG as the PCM to the PBAT matrix was determined through analyses of mechanical properties and morphological appearance. Mechanical property analysis indicated improved tensile strength with the inclusion of APTES-treated AlN particles. DMA revealed increased stiffness in the composites, while LFA showed a significant enhancement in thermal conductivity, approximately 325% higher than that of the base 20PCM−PBAT composite. Additionally, the latent heat of the fabricated composites was found to be improved compared to neat PBAT. Specifically, the 20PCM−PBAT−30F composite exhibited a latent heat of 122 J/g, which is nearly equivalent to that of neat PEG (PCM) but twice that of PBAT alone. Overall, our findings highlight the efficacy of IPDI- and APTES-treated CNT and AlN particles, respectively, in enhancing the latent heat, thermal, and mechanical properties of polymer composites. These enhancements pave the way for their broader application in various fields, leveraging the improved performance characteristics of these composites for advanced thermal management and energy storage solutions.

■ ASSOCIATED CONTENT

Supporting Information

The Supporting Information is available free of charge at https://pubs.acs.org/doi/10.1021/acsomega.4c07480.

TEM images of IPDI-treated CNT and EDS analysis results of IPDI-treated CNT including the elements present in NCO and CNT (Figure S1); IPDI-treated AlN particles and EDS analysis (Figure S2); leakage tests of various samples investigated at different temperatures above the melting point of PEG (Figure S3); and stress−strain diagram, tensile strength, and elongation at break of various PCM−PBAT−filler composites (Figure S4) (PDF)

■ AUTHOR INFORMATION

Corresponding Author

Jooheon Kim − *Department of Intelligent Energy and Industry, Chung-Ang University, Seoul 06974, Republic of Korea; School of Chemical Engineering and Material Science, Chung-Ang University, Seoul 06974, Republic of Korea;* orcid.org/0000-0002-6644-7791; Phone: +82-2-820-5763; Email: jooheonkim@cau.ac.kr; Fax: +82-2-812-3495

Authors

Eyob Wondu − *Department of Intelligent Energy and Industry, Chung-Ang University, Seoul 06974, Republic of Korea*

Wondu Lee − *School of Chemical Engineering and Material Science, Chung-Ang University, Seoul 06974, Republic of Korea*

Minsu Kim − *School of Chemical Engineering and Material Science, Chung-Ang University, Seoul 06974, Republic of Korea*

Dabin Park − *Department of Mechanical and Aerospace Engineering, University of California, Irvine, Irvine, California 92679, United States*

Complete contact information is available at: https://pubs.acs.org/10.1021/acsomega.4c07480

Author Contributions

‖E.W. and W.L. equally contributed to this work.

Notes

The authors declare no competing financial interest.

■ ACKNOWLEDGMENTS

This research was supported by the National Research Foundation of Korea (NRF) grant funded by the Korea government (MSIT) (RS-2024-00448445) and supported by the MSIT (Ministry of Science and ICT), Korea, under the ITRC (Information Technology Research Center) support program (IITP-2023-2020-0-01655) supervised by the IITP (Institute of Information & Communications Technology Planning & Evaluation).

REFERENCES

(1) Schinazi, G.; Price, E. J.; Schiraldi, D. A. Fire testing methods of bio-based flame-retardant polymeric materials. *Bio-Based Flame-Retardant Technol. Polym. Mater.* **2022**, *59*, 61−95.

(2) Song, S.; Zhao, T.; Zhu, W.; Qiu, F.; Wang, Y.; Dong, L. Natural Microtubule-Encapsulated Phase-Change Material with Simultaneously High Latent Heat Capacity and Enhanced Thermal Conductivity. *ACS Appl. Mater. Interfaces* **2019**, *11*, 20828−20837.

(3) Wu, S.; Zhou, Y.; Gao, W.; Zhang, Z.; Liu, A.; Cai, R.; et al. Preparation and properties of shape-stable phase change material with enhanced thermal conductivity based on SiC porous ceramic carrier made of iron tailings. *Appl. Energy* **2024**, *355*, No. 122256.

(4) Lee, W.; Seo, M.; Kim, J. Ultra-high thermal conductivity and mechanical properties of a paraffin composite as a thermal conductive phase change materials for novel heat management. *Compos. Sci. Technol.* **2022**, *220*, No. 109282.

(5) Chibani, A.; Dehane, A.; Merouani, S. The sono-PCM reactors: A new approach for recovering the heat dissipated from ultrasonic reactors using a phase change material. *Int. J. Heat Mass Transfer* **2023**, *215*, No. 124505.

(6) Xu, C.; Zhang, H.; Fang, G. Review on thermal conductivity improvement of phase change materials with enhanced additives for thermal energy storage. *J. Energy Storage* **2022**, *51*, No. 104568.

(7) Jia, X.; Li, Q.; Ao, C.; Hu, R.; Xia, T.; Xue, Z.; et al. High thermal conductive shape-stabilized phase change materials of polyethylene glycol/boron nitride@chitosan composites for thermal energy storage. *Composites, Part A* **2020**, *129*, No. 105710.

(8) Sarcinella, A.; de Aguiar, J. L. B.; Jesus, C.; Frigione, M. Thermal properties of PEG-based form-stable Phase Change Materials (PCMs) incorporated in mortars for energy efficiency of buildings. *J. Energy Storage* **2023**, *67*, 107545.

(9) Dutta, P. P.; Saxena, V.; Kumar, A.; Sahu, S. K. Investigation of finned heat sinks with PEG-6000/EG and PEG-6000/MWCNT composite phase change material for thermal management application. *J. Energy Storage* **2023**, *70*, No. 108057.

(10) Sun, J.; Zhao, J.; Zhang, W.; Xu, J.; Wang, B.; Wang, X.; et al. Composites with a Novel Core−shell Structural Expanded Perlite/Polyethylene glycol Composite PCM as Novel Green Energy Storage Composites for Building Energy Conservation. *Appl. Energy* **2023**, *330*, No. 120363.

(11) Lin, Y.; Jia, Y.; Alva, G.; Fang, G. Review on thermal conductivity enhancement, thermal properties and applications of phase change materials in thermal energy storage. *Renewable Sustainable Energy Rev.* **2018**, *82*, 2730−2742.

(12) Li, Y.; Zhang, W.; Sun, J.; Fang, X.; Wang, B.; Li, F.; et al. A route of polyethylene glycol-based phase change heat storage wood with AlN as the thermal conductive filler. *Wood Sci. Technol.* **2023**, *57*, 717−739.

(13) Stonehouse, A.; Abeykoon, C. Thermal properties of phase change materials reinforced with multi-dimensional carbon nanomaterials. *Int. J. Heat Mass Transfer* **2022**, *183*, No. 122166.

(14) Wong, T. L.; Vallés, C.; Nasser, A.; Abeykoon, C. Effects of boron-nitride-based nanomaterials on the thermal properties of composite organic phase change materials: A state-of-the-art review. *Renewable Sustainable Energy Rev.* **2023**, *187*, 113730.

(15) Wong, T. L.; Ma, K.; Abeykoon, C. Enhancing the thermal performance of polyethylene glycol phase change material with carbon-based fillers. *Int. J. Heat Mass Transfer* **2024**, *220*, 124919.

(16) Zhang, X.; Zheng, J.; Fang, H.; Zhang, Y.; Bai, S.; He, G. Al2O3/graphene reinforced bio-inspired interlocking polyurethane composites with superior mechanical and thermal properties for solid propulsion fuel. *Compos. Sci. Technol.* **2018**, *167*, 42−52.

(17) Zhou, W.; Kou, Y.; Yuan, M.; Li, B.; Cai, H.; Li, Z.; et al. Polymer composites filled with core@double-shell structured fillers: Effects of multiple shells on dielectric and thermal properties. *Compos. Sci. Technol.* **2019**, *181*, 107686.

(18) Wondu, E.; Lule, Z. C.; Kim, J. Fabrication of high dielectric properties and higher thermal conductivity thermoplastic polyurethane composites with CNT-covered SrTiO3. *Polym. Test.* **2022**, *110*, No. 107576.

(19) Wondu, E.; Lule, Z. C.; Kim, J. Improvement of dielectric constant and mechanical properties of thermoplastic polyurethanes using surface modified strontium titanate. *Polym. Compos.* **2023**, *44*, 168−177.

(20) Kim, K.; Kim, M.; Kim, J. Enhancement of the thermal and mechanical properties of a surface-modified boron nitride-polyurethane composite. *Polym. Adv. Technol.* **2014**, *25*, 791−798.

(21) Chi, Q.; Zhang, X.; Wang, X.; Zhang, C.; Zhang, Y.; Tang, C.; et al. High thermal conductivity of epoxy-based composites utilizing 3D porous boron nitride framework. *Compos. Commun.* **2022**, *33*, No. 101195.

(22) Lule, Z.; Kim, J. Surface Modification of Aluminum Nitride to Fabricate Thermally Conductive poly(Butylene Succinate) Nanocomposite. *Polymers* **2019**, *11*, 148.

(23) Du, F. P.; Li, J. J.; Fu, P.; Wu, Y. G.; Liao, G. Y.; Zhang, Y. F.; Luo, S. Enhanced thermal conductivity of poly(L-lactide) composites with synergistic effect of aluminum nitride and modified multi-walled carbon nanotubes. *Fullerenes, Nanotubes, Carbon Nanostruct.* **2016**, *24*, 667−673.

(24) Wondu, E.; Lule, Z.; Kim, J. Thermal conductivity and mechanical properties of thermoplastic polyurethane-/silane-modified Al2O3 composite fabricated via melt compounding. *Polymers* **2019**, *11*, 1103.

(25) Wondu, E.; Lule, Z. C.; Kim, J. Improvement of dielectric properties and thermal conductivity of TPU with alumina-encapsulated rGO. *Polym. Test.* **2021**, *102*, 107322.

(26) Raghu, A. V.; Lee, Y. R.; Jeong, H. M.; Shin, C. M. Preparation and physical properties of waterborne polyurethane/functionalized graphene sheet nanocomposites. *Macromol. Chem. Phys.* **2008**, *209*, 2487−2493.

(27) Parida, S.; Parida, R. K.; Parida, B. N.; Padhee, R.; Nayak, N. C. Structural, thermal and dielectric behaviour of exfoliated graphite nanoplatelets (xGnP) filled EVA/EOC blend composites. *Mater. Sci. Eng. B* **2022**, *275*, No. 115497.

(28) Zhao, Z. B.; Liu, J. D.; Du, X. Y.; Wang, Z. Y.; Zhang, C.; Ming, S. F. Fabrication of silver nanoparticles/copper nanoparticles jointly decorated nitride flakes to improve the thermal conductivity of polymer composites. *Colloids Surf., A* **2022**, *635*, No. 128104.

(29) Liu, Y.; Tao, R.; Chen, S.; Wu, K.; Zhong, Z.; Tu, J.; et al. A novel polyurethane-LiF artificial interface protective membrane as a promising solution towards high-performance lithium metal batteries. *J. Power Sources* **2020**, *477*, 228694.

(30) Wondu, E.; Lule, Z. C.; Kim, J. Fabrication of thermoplastic polyurethane composites with a high dielectric constant and thermal conductivity using a hybrid filler of CNT@BaTiO3. *Mater. Today Chem.* **2023**, *27*, No. 101287.

(31) Wondu, E.; Kim, J. Improvement of thermo-mechanical and dielectric properties of poly(lactic acid) and thermoplastic polyurethane blend composites using a graphene and BaTiO3 filler. *Polym. Eng. Sci.* **2024**, *64*, 207−217.

(32) Luo, F.; Wu, K.; Guo, H.; Zhao, Q.; Lu, M. Anisotropic thermal conductivity and flame retardancy of nanocomposite based on mesogenic epoxy and reduced graphene oxide bulk. *Compos. Sci. Technol.* **2016**, *132*, 1−8.

(33) Wattanakul, K.; Manuspiya, H.; Yanumet, N. The adsorption of cationic surfactants on BN surface: Its effects on the thermal conductivity and mechanical properties of BN-epoxy composite. *Colloids Surf., A* **2010**, *369*, 203−210.

(34) Mirkhani, S. A.; Zeraati, A. S.; Aliabadian, E.; Naguib, M.; Sundararaj, U. High Dielectric Constant and Low Dielectric Loss via Poly(vinyl alcohol)/Ti3C2Tx MXene Nanocomposites. *ACS Appl. Mater. Interfaces* **2019**, *11*, 18599−18608.

(35) Lule, Z. C.; Wondu, E.; Kim, J. Highly rigid, fire-resistant, and sustainable polybutylene adipate terephthalate/polybutylene succinate composites reinforced with surface-treated coffee husks. *J. Cleaner Prod.* **2021**, *315*, No. 128095.

https://doi.org/10.1021/acsomega.4c07480
ACS Omega 2024, 9, 49557−49565